









RESEARCH ARTICLE | JUNE 26 2023

Picosecond magneto-optic thermometry measurements of nanoscale thermal transport in AlN thin films

Frank Angeles ; Samreen Khan ; Victor H. Ortiz ; Mingfei Xu ; Shisong Luo; Dinusha Herath Mudiyansele ; Houqiang Fu ; Yuji Zhao; Richard B. Wilson  

 Check for updates

APL Mater 11, 061127 (2023)

<https://doi.org/10.1063/5.0149651>



View
Online



Export
Citation

CrossMark

Articles You May Be Interested In

Magnetothermopower and magnetoresistivity of PtCo

Journal of Applied Physics (August 2008)

Magnetic Properties of an Equi-Atomic PtCo Single Crystal Having a [111] Orientation

Journal of Applied Physics (November 2003)

Investigation of interaction mechanisms in nanocomposite PtCo permanent magnetic alloy

Journal of Applied Physics (April 2011)



Optimize
Your
Research

New Vacuum Gauge Provides
More Process Control
and Operational Reliability



PFEIFFER  VACUUM

Picosecond magneto-optic thermometry measurements of nanoscale thermal transport in AlN thin films

Cite as: APL Mater. 11, 061127 (2023); doi: 10.1063/5.0149651

Submitted: 7 March 2023 • Accepted: 25 May 2023 •

Published Online: 26 June 2023



View Online



Export Citation



CrossMark

Frank Angeles,¹ Samreen Khan,¹ Victor H. Ortiz,¹ Mingfei Xu,² Shisong Luo,²
Dinusha Herath Mudiyansele,³ Houqiang Fu,³ Yuji Zhao,² and Richard B. Wilson^{1,a)}

AFFILIATIONS

¹Mechanical Engineering, Materials Science and Engineering, University of California, Riverside, California 92521, USA

²Department of Electrical and Computer Engineering, Rice University, Houston, Texas 77005, USA

³School of Electrical, Computer and Energy Engineering, Arizona State University, Tempe, Arizona 85287, USA

^{a)}Author to whom correspondence should be addressed: rwilson@ucr.edu

ABSTRACT

The thermal conductivity Λ of wide bandgap semiconductor thin films, such as AlN, affects the performance of high-frequency devices, power devices, and optoelectronics. However, accurate measurements of Λ in thin films with sub-micrometer thicknesses and $\Lambda > 100 \text{ W m}^{-1} \text{ K}^{-1}$ is challenging. Widely used pump/probe metrologies, such as time-domain thermoreflectance (TDTR) and frequency-domain thermoreflectance, lack the spatiotemporal resolution necessary to accurately quantify thermal properties of sub-micrometer thin films with high Λ . In this work, we use a combination of magneto-optic thermometry and TiN interfacial layers to significantly enhance the spatiotemporal resolution of pump/probe thermal transport measurements. We use our approach to measure Λ of 100, 400, and 1000 nm AlN thin films. We coat AlN thin films with a ferromagnetic thin-film transducer with the geometry of $(1 \text{ nm-Pt}/0.4 \text{ nm-Co})_{\times 3}/(2 \text{ nm-TiN})$. This PtCo/TiN transducer has a fast thermal response time of $< 50 \text{ ps}$, which allows us to differentiate between the thermal response of the transducer, AlN thin film, and substrate. For the 100, 400, and 1000 nm thick AlN films, we determine Λ to be 200 ± 80 , 165 ± 35 , and $300 \pm 70 \text{ W m}^{-1} \text{ K}^{-1}$, respectively. We conclude with an uncertainty analysis that quantifies the errors associated with pump/probe measurements of thermal conductivity, as a function of transducer type, thin-film thermal conductivity, and thin-film thickness. Time resolved magneto-optic Kerr effect experiments can measure films that are three to five times thinner than is possible with standard pump/probe metrologies, such as TDTR. This advance in metrology will enable better characterization of nanoscale heat transfer in high thermal conductivity material systems like wide bandgap semiconductor heterostructures and devices.

© 2023 Author(s). All article content, except where otherwise noted, is licensed under a Creative Commons Attribution (CC BY) license (<http://creativecommons.org/licenses/by/4.0/>). <https://doi.org/10.1063/5.0149651>

I. INTRODUCTION

Homo- and hetero-epitaxial layers of wurtzite AlN are an important class of materials for power electronics,¹ radio frequency (RF) electronics, and optoelectronics.^{2,3} The high power density experienced by such devices leads to high operating temperatures.⁴ High device temperatures limit device performance and reliability.⁵ Therefore, part of the appeal of AlN for such devices is its high thermal conductivity (Λ). Bulk crystals of wurtzite AlN have reported values for Λ at room temperature between 300 and 340 W/(mK).^{6,7}

Characterizing Λ in nanoscale structures, such as AlN thin films, requires that the heat be spatially confined to the region of interest. One way to do this is to thermally isolate the structure of interest using nanofabrication techniques.⁸ This nanofabrication approach is often used to study Λ of two-dimensional (2D) materials⁹ and nanowires¹⁰ but is rarely used to study thin semiconductor films. Thin films are generally studied with transient pump/probe techniques.^{11,12} In transient pump/probe techniques, heat is confined spatially as a result of the short experimental time scales. The distance L that heat diffuses in time t is determined by the thermal

diffusivity α , $L \approx (\alpha t)^{1/2}$. By measuring the thermal response on microsecond to nanosecond time scales, time-domain thermoreflectance (TDTR) and frequency-domain thermoreflectance (FDTR) experiments are able to quantify thermal transport on micrometer and submicrometer length scales. The minimum length scale that a TDTR or FDTR experiment can probe is determined by α of the material of interest and the temporal resolution of the experiment.

Before conducting TDTR and FDTR experiments, the samples are coated with a metal film to serve as an optical transducer.¹² This optical transducer absorbs heat from the laser, and its thermoreflectance is used as an optical thermometer. The speed with which the temperature of this transducer layer can respond to changes in the temperature of the adjacent sample determines the temporal resolution of the experiment.¹³

The thermal response time of the metal transducer is $\tau \approx hC/G$, where h is the metal transducer's total thickness, C is its average volumetric heat capacity, and G describes how good the thermal contact with the sample is. Typical values for these parameters are $h = 80$ nm, $C = 2.5$ MJ m⁻³ K⁻¹, and $G = 100$ MW m⁻² K⁻¹. Therefore, the thermal response time is typically of the order of $\tau \approx 2$ ns. As a result, for a material with high thermal diffusivity like AlN with $\alpha \approx 1.4 \times 10^{-4}$ m² s⁻¹, spatial resolution of TDTR and FDTR is limited to length scales greater than $L \approx 500$ nm.

One way to improve spatiotemporal resolution is to decrease the thermal response time of the transducer τ by decreasing the film thickness h . Experiments that rely on thermoreflectance thermometry cannot do this because h must be large enough that the transducer is completely optically opaque.¹³ If h is not large enough, i.e., $h > 40$ nm, the reflected probe beam will contain spurious thermoreflectance signals generated by temperature-induced changes in the optical constants of the sample.¹⁴ This is problematic because the thermal models used to analyze TDTR and FDTR data assume that thermoreflectance signals are a measure of the surface temperature only. Several recent studies have explored TDTR without a metal transducer.^{15,16} However, without a metal transducer, heat is deposited across the micron-scale optical penetration depth of semiconductors, which affects spatial resolution.¹⁶ Furthermore, the interpretation of signals is complicated by the effect of photoexcited carriers.¹⁷

Time-resolved magneto-optic Kerr effect (TR-MOKE) measurements have emerged as an alternative to TDTR for measurements that require a thin transducer.^{13,18} TR-MOKE is a pump/probe method similar to TDTR. However, TR-MOKE uses a ferromagnetic metal as the transducer. Rather than measuring temperature-induced changes in the intensity of the reflected probe beam, TR-MOKE experiments measure temperature-induced changes in the polarization of the reflected probe beam.¹⁹ The Kerr rotation of the magnetic material can be used as a thermometer because it originates from the magnetism of the transducer, which depends on the temperature. Since the signal is magnetic in origin, it originates from only the magnetic transducer layer even when the film is semi-transparent.¹³

Several recent thermal transport studies that required small h transducers have made use of TR-MOKE. Kimling *et al.* used TR-MOKE to study transport at interfaces between Pt and amorphous SiO₂.¹³ TR-MOKE has also been used to measure in-plane thermal conductivity of anisotropic bulk crystals^{13,20} and quasi-2D

materials.^{18,21,22} For in-plane thermal conductivity measurements, it is advantageous to minimize the in-plane heat current carried by the metal transducer, which scales with $h\Lambda_{\text{metal}}$.

In this work, we use TR-MOKE to study the cross-plane Λ of AlN thin films. To maximize the spatiotemporal resolution of our experiment, we use a thin magnetic multilayer as the transducer with the following geometry: [1 nm-Pt/0.4 nm-Co]_{x3}/[2 nm-TiN]. The Pt/Co multilayer has perpendicular magnetic anisotropy and a large polar magneto-optic Kerr effect. The TiN interfacial layer ensures good thermal contact between the transducer and the AlN thin film. We use TiN because TiN interfaces have some of the highest reported G values of any metal, i.e., $G > 400$ MW m⁻² K⁻¹.^{23,24} As a result of a small h and high G , the PtCo/TiN transducer has a thermal response time of ~ 50 ps. For comparison, the thermal response times of an 80 nm Al film and 40 nm TiN film are ~ 1500 ps and ~ 250 ps

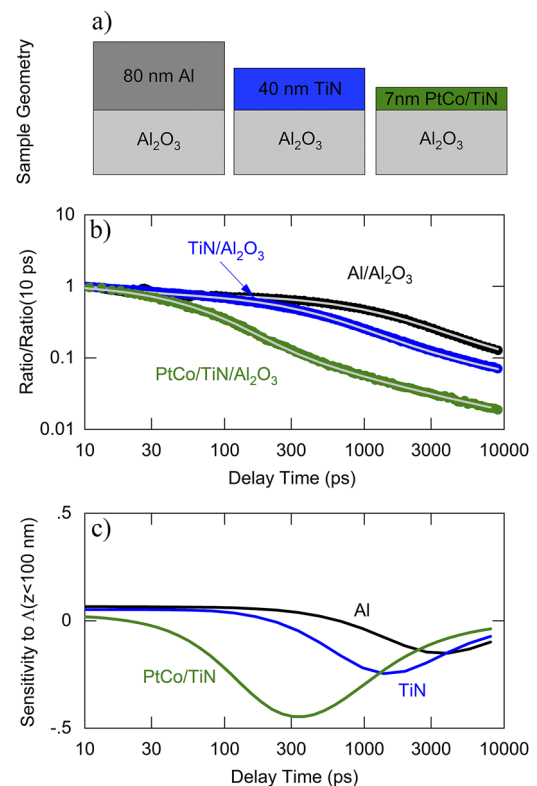


FIG. 1. Comparison of the thermal response times of three types of metal transducers. (a) Schematic of sample geometry for transducer characterization. The PtCo/TiN transducer is a multilayer with a geometry of [1 nm Pt/0.4 nm Co]_{x3}/[2 nm TiN]. (b) Time-domain thermoreflectance data for Al and TiN transducers (black and blue markers) and time-resolved magneto-optic Kerr-effect data for the PtCo/TiN transducer (green markers). Gray lines are thermal model predictions with best-fit values for the interface conductance of 120, 500, and 500 MW/m² K for the Al, TiN, and PtCo/TiN transducer, respectively. The thermal response time of the transducer decreases with thickness. It also decreases as the interfacial thermal conductance increases. (c) Calculated sensitivity of the experimental signals in (a) to the near surface region of the sapphire substrate. Sensitivity to the top 100 nm of the sapphire increases as the thermal response time of the transducer decreases.

(see Fig. 1). The fast thermal response of the PtCo/TiN transducer allows us to separate the thermal response of the AlN thin films from that of the interface and substrate.

We measure the thermal conductivity of three AlN thin films with thicknesses of 1, 0.4, and 0.1 μm . The 0.4 and 1 μm AlN films were metalorganic chemical vapor deposition (MOCVD) grown epilayers on sapphire. The 0.1 μm AlN thin film is an n-type Si doped AlN film that was MOCVD grown homoepitaxially on an AlN substrate. For 400 and 1000 nm thick AlN films, we determine Λ to be 165 ± 35 and $300 \pm 70 \text{ Wm}^{-1} \text{ K}^{-1}$, respectively. For the 100 nm n-type AlN film, we determine that the thermal conductivity to be $200 \pm 80 \text{ Wm}^{-1} \text{ K}^{-1}$. We conclude our study by theoretically evaluating how the thermal response time affects measurement accuracy and resolution for different types of materials.

II. METHODS

A. Sample preparation

The homoepitaxial AlN layer was grown by metalorganic chemical vapor deposition (MOCVD) on a single crystal AlN substrate with a dislocation density of $<10^3 \text{ cm}^{-2}$. Trimethylaluminum (TMAl), ammonia (NH_3), and silane (SiH_4) were used as precursors for Al, N, and n-type Si dopant, respectively. The carrier gas was hydrogen (H_2) and the growth temperature was $\sim 1100^\circ\text{C}$. A 100 nm Si-doped n-type AlN epilayer with a Si doping concentration of $1 \times 10^{19} \text{ cm}^{-3}$ was homoepitaxially grown on top of 550 nm undoped AlN buffer layer on single crystal AlN substrate. The resistivity of the Si-doped AlN film was $\sim 10 \Omega \text{ cm}$. High-resolution x-ray diffraction (HRXRD) and atomic force spectroscopy (AFM) measurements indicate that the n-type AlN film had excellent crystal quality with defect density on the order of 10^3 cm^{-2} and low surface roughness of $<1 \text{ nm}$. Additional details about the growth can be found elsewhere.^{25,26}

The two other AlN thin films that we studied were MOCVD grown epilayers on sapphire purchased from commercial vendors. The 1 μm AlN film was grown on (0001) sapphire by MOCVD (DOWA Electronics Materials). The surface roughness was measured with AFM to be 0.24 nm. The 0.4 μm AlN thin film was grown on (0001) sapphire by MOCVD (Kyma Technologies). The surface roughness was measured with AFM to be 1.6 nm. AFM and transmission electron microscopy (TEM) images are provided in the supplementary material Figs. S1–S3.

The AlN films were coated with TiN via reactive DC magnetron sputtering using an AJA Orion series sputtering system. To ensure a base vacuum pressure $<3 \times 10^{-8}$ Torr before TiN deposition, the chamber was baked at 100°C for 12 h. Additionally, liquid nitrogen was circulated through coils inside that chamber during the sputtering process. During sputtering, the pressure was increased to 1.3×10^{-3} Torr by introducing a mixture of Ar and N_2 with partial pressures of 6×10^{-4} and 7×10^{-4} Torr, respectively. The TiN seed layer was deposited at a temperature of 575°C . The initial thickness of the TiN layer is $\sim 4 \text{ nm}$. Further details of how TiN was grown can be found elsewhere.²³

Following the deposition of TiN, the substrates were allowed to cool to room temperature under a high vacuum of $\sim 3 \times 10^{-8}$ Torr. Once the substrates reached room temperature, the pressure was raised to 3.5 mTorr by introducing only high purity Ar via an air

mass flow sensor. The substrates were then etched with an RF sputter at 3.5 mTorr at a power of 45 W for 5 min. This removes $\sim 2 \text{ nm}$ of TiN. As we discuss more below, the sputter etch of the TiN surface is necessary to ensure good thermal contact between the Pt/Co multilayer and the TiN layer. Then, the Pt/Co metal multilayer is sputter deposited. The final multilayer geometry is [1 nm-Pt/0.4 nm-Co]/[2 nm-TiN].

During deposition of the transducer on the AlN samples, a sapphire substrate was added to the chamber. TR-MOKE measurements of the sapphire sample are used to verify the thickness of the transducer layer. Furthermore, to compare the thermal response time between different types of transducers, we also prepared sapphire samples with 80 nm Al and 40 nm TiN.

B. Experimental methods

We used TDTR and TR-MOKE experiments to measure the thermal conductivity of the three aluminum nitride films. Details about our pump/probe system for TDTR and TR-MOKE measurements are described in Ref. 27. In all current experiments, the pump and probe beams are focused down on the sample via a $10\times$ objective lens to a laser spot size is $\sim 7.5 \mu\text{m}$.

The pump beam is modulated at a frequency of 10.7 MHz by an electric optical modulator (EOM). Temperature-induced changes in intensity and polarization of the reflected probe beam are monitored via lock-in detection at 10.7 MHz. The signal of interest is the ratio of the in-phase and out-of-phase lock-in signals, $R = V_{in}/V_{out}$.¹¹ These signals are collected as a function of time delay between the pump and probe beams. All measurements were made at room temperature. Pump and probe powers are set to keep the steady-state temperature increase of the system $<5 \text{ K}$. The pump fluence was $\sim 1.4 \text{ J/m}^2$. A multilayer optical calculation predicts that the PtCo/TiN transducer has an absorption of ≈ 0.24 . So, the per pulse temperature increase in our experiments is less than 20 K.

We analyze the ratio signal using a multilayer analytical solution to the heat diffusion equation in cylindrical coordinates.¹¹ The thermal model takes the thermal properties and thicknesses of each layer as inputs and then produces a prediction for the ratio of the in-phase and out-phase temperature responses. The important model inputs are the transducers metal film thickness h and heat capacity C , the interface conductance G between TiN and the AlN, the thickness of the AlN film layer, and the substrate's heat capacity and thermal conductivity. The thickness of the metal transducer is obtained from a control sample of sapphire that was sputter deposited at the same time (see the supplementary material). The transducer and substrate heat capacity and thermal conductivity are set on the basis of literature values. The AlN nitride film thickness for the commercial CVD wafers was obtained from TEM imaging or laser interferometry. The only two of the thermal model parameters not fixed based on literature values are the interface conductance G between the transducer and AlN, and the thermal conductivity Λ of the AlN film. We treat these two values as fit parameters and adjust the values until the thermal model predictions for the ratio agree with our experimental measurement.

For thermal modeling of the 100 nm n-type AlN sample, the sample stack has three layers: 100 nm Si-doped AlN, a 550 nm undoped AlN buffer layer, and an AlN substrate. For thermal modeling, we assumed the buffer layer and substrate to have the same

thermal properties. In other words, we lump the buffer layer and substrate together. As discussed in the Results section, this assumption yields a best-fit value for Λ of the combined layer that agrees with the values in the literature for bulk single crystals of AlN. Therefore, the assumption to lump these two layers together is reasonable.

There is a range of values for Λ and G that we can input into the model that result in reasonable agreement with the data. To determine this range, we perform a contour analysis like the kind described in Refs. 28 and 29. We calculate the root mean square percentage error between the model and the data for a matrix of Λ and G values. The RMSE value of <6.5% is set as the limit for reasonable agreement between the model and the data. Further details for the RMSE analysis can be found in the supplementary material Fig. S4.

III. THERMAL RESPONSE TIME OF TRANSDUCER LAYER

To examine the thermal response time of different types of metal film transducers, we compare TDTR and TR-MOKE signals for 80 nm of Al, 40 nm of TiN, and 7 nm of PtCo/TiN transducers on sapphire. These results are shown in Fig. 1. As expected, the thermal response time scales with the thickness of the transducer. The thermal response time we observe is 1600, 200, and 38 ps for Al, TiN, and PtCo/TiN, respectively. Here, we defined the thermal response time to be time delays at which the ratio signal drops by a factor of $1/e$.

The lines in Fig. 1(a) are predictions for the ratio with the sapphire thermal conductivity and the transducer/sapphire interface conductance G treated as fit parameters. The thermal conductivities that produce the best fit for the three datasets are $\Lambda = 38 \pm 3 \text{ Wm}^{-1} \text{ K}^{-1}$, $\Lambda = 38 \pm 3 \text{ Wm}^{-1} \text{ K}^{-1}$, and $\Lambda = 38 \pm 2 \text{ Wm}^{-1} \text{ K}^{-1}$ for Al, TiN, and PtCo/TiN, respectively. Both TiN transducers have similarly high values for the interface conductance of $G = 500 \pm 50 \text{ MW m}^{-2} \text{ K}^{-1}$. The 80 nm Al transducer has an interface conductance value of $G = 120 \pm 10 \text{ MW m}^{-2} \text{ K}^{-1}$.

The thermal response time of the transducer has a strong effect on the sensitivity of our measurement to the thermal conductivity of the sapphire in the near-surface region. To show this, we performed sensitivity calculations; see Fig. 1(c). We define the sensitivity parameter as the logarithmic derivative of the experimental signal with respect to a thermal property.³⁰ The sensitivity describes how much a change in the value of a thermal property will change the experimental signal. For example, a sensitivity of 0.5 to the thermal conductivity of sapphire implies that 10% increase in the thermal conductivity of sapphire would change the experimental signal by +5%. Our calculations show that the peak sensitivity to $\Lambda_{\text{sapphire}}$ ($z < 100 \text{ nm}$) is -0.15 , -0.25 , and -0.4 for the Al, TiN, and PtCo/TiN transducers, respectively. Additional information on how the sensitivity of TDTR and TR-MOKE signals depend on transducer type is provided in Fig. S5.

In dielectric materials at room temperature, heat is carried by phonons with frequencies in the terahertz (THz) range. Phonon lifetimes at room temperature are typically one tenth to one hundred of the phonon's precessional period,³¹ i.e., 1–10 ps. Therefore, we do not expect nonequilibrium effects to be important in our experiments, which have important time-scales longer than 50 ps.

IV. THERMAL RESISTANCE OF THE METAL TRANSDUCER

In our discussion above about transducer thermal response times τ , we neglected the effect of the thermal resistance of the metal transducer. We now consider that effect. Any thermal resistances internal to the metal transducer will add in series with the transducer/sample interface resistance and slow the thermal response time of the transducer. With the effect of thermal resistance of the transducer included, the thermal response time can be approximated as $\tau \approx hC(R_{\text{metal}} + 1/G)$. Here, R_{metal} is the total internal thermal resistance of the transducer. R_{metal} includes h/Λ and the resistance of any internal metal/metal interfaces. h/Λ for all three transducers is reasonably small and can therefore be neglected. However, the PtCo/TiN transducer contains many internal metal/metal interfaces. Of particular concern is the Co/TiN interface, as the Co is sputtered $\sim 3 \text{ h}$ after the TiN layer to accommodate the different deposition temperatures. Our initial efforts to prepare PtCo/TiN transducers with fast thermal response times were unsuccessful. This failure was likely caused by a large value for R_{metal} . To address this challenge, we conducted a set of experiments to explore how our synthesis procedure impacted the TiN/Co metal/metal interface conductance.

In prior work,²⁸ we showed that a combination of front/front and front/back TDTR experiments allows the metal/metal interface conductance to be measured. To characterize how G of the TiN/Co interface depends on the synthesis procedures, we follow the same experimental procedure as described in Ref. 28. We

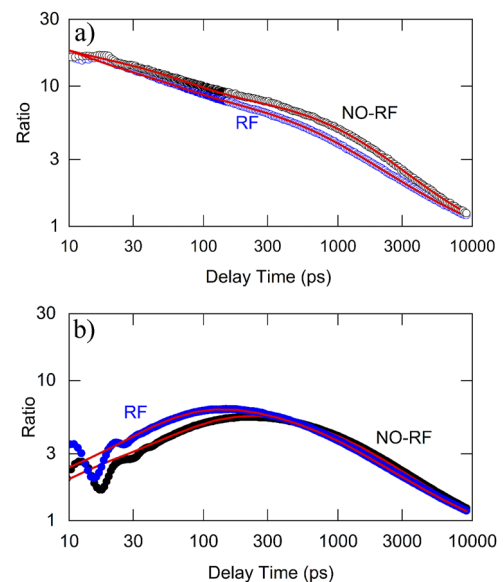


FIG. 2. TDTR data for Al/Co/TiN trilayer on sapphire. Black and blue markers are data for trilayers prepared with no RF, and with 300 s of RF sputtering prior to Co layer deposition, respectively. The red lines are model predictions with $G \approx 900 \text{ MW m}^{-2} \text{ K}^{-1}$ (black marker data) and $G > 5000 \text{ MW m}^{-2} \text{ K}^{-1}$ (blue marker data). The data in (a) was collected with pump and probe beams in a front-front configuration, i.e., pump and probe are both incident on the Al surface. The data in (b) was collected with pump and probe beams in a front-back configuration, i.e., the pump was focused through the sapphire onto the TiN/sapphire interface and the probe was focused on the Al surface.

prepared two sets of [20 nm-Al/30 nm-Co/30 nm-TiN] trilayers. The Al layer was included to overcome the poor thermorefectance of Co. For one sample, we RF sputter-etched the TiN surface immediately prior to Co deposition. The other sample was not etched with an RF sputter. We performed two sets of TDTR experiments on both samples; see Fig. 2. In one set of experiments, the pump beam irradiated the Al surface (front/front measurements). In the other set of experiments, the pump beam excited the TiN/sapphire interface (front/back experiments). In both sets of experiments, the probe beam was reflected from the Al surface. Therefore, the signal that we measure is proportional to the Al surface temperature.

We analyze the data with a two-temperature model,²⁸ and fit the data for the electron interface conductance between the Co and TiN layers. We observe that for the RF sputter etch sample, the TiN/Co interface conductance is larger than $5 \text{ GW m}^{-2} \text{ K}^{-1}$. However, if we do not sputter etch the TiN surface prior to Co deposition, the interface conductance is $\sim 900 \text{ MW m}^{-2} \text{ K}^{-1}$. We credit the low conductance to oxide formation that results during the $\sim 3 \text{ h}$ it takes for the sample to cool in vacuum from (of 575°C) to room temperature. In the experiments shown below, an RF sputter etch step was included in the synthesis of the PtCo/TiN transducer.

V. TRANSDUCER THICKNESS REQUIREMENT FOR OPAQUE SUBSTRATE

The thermal model we use to analyze data assumes that heat is solely absorbed at the surface of the metal.¹¹ This assumption will not be suitable for thin transducers deposited on opaque samples such as silicon. To test how thick the transducer needs to be for non-transparent vs transparent samples, we performed a series of TR-MOKE measurements of silicon and 300 nm SiO_2/Si with varied transducer thicknesses. These results are summarized in Fig. 3.

Silicon has an indirect bandgap of 1.1 eV and is not transparent at our laser energy of 1.56 eV. Alternatively, SiO_2 has a bandgap of 8.4 eV and therefore is transparent. We deposited Pt/Co transducers with thicknesses that varied between 7 and 35 nm. In Fig. 3, we compare the measured ratio at a time delay of 20 ps to the thermal model predictions. For thin transducers deposited on silicon, we observed significant deviations between experiment and the thermal model predictions. We attribute this discrepancy to opti-

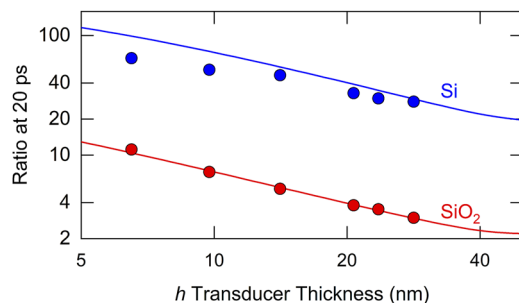


FIG. 3. TR-MOKE signals as a function of transducer thickness for a transparent SiO_2 vs opaque Si sample. Experimental measurements of silicon with transducers less than 30 nm disagree with thermal model predictions (lines). The thermal model assumes heat is deposited at the surface of the metal, and no heat is absorbed by the substrate.

cal heating of silicon, which the thermal model does not include. In contrast, the experimental observations and model predictions are in good agreement for samples deposited on SiO_2 . We conclude that a transducer thickness of 30 nm is required for opaque films and/or substrates, and no minimum thickness is required for transparent samples. AlN's wide bandgap means all the samples of interest are transparent and do not require a 30 nm thick transducer.

VI. THERMAL CONDUCTIVITY OF ALN THIN FILMS

We now turn our attention to the main goal of our study: measurements of the thermal conductivity of sub-micrometer AlN layers. In Fig. 4, we compare TDTR and TR-MOKE measurements of 0.4 μm thick AlN epilayer on sapphire with different transducers. In Fig. 5, we summarize the results of TR-MOKE measurements of the 1, 0.4, and 0.1 μm thick AlN layers. Figures 4 and 5 are the primary results of this study. Additionally, TR-MOKE results for sapphire are provided in Fig. S6.

The central hypothesis of our study is that transducers with short thermal response times allow for more accurate measurements of thin-film thermal conductivity. This hypothesis is corroborated by comparing the TDTR and TR-MOKE measurements of the 0.4 μm AlN epilayer. Figure 4(a) shows the TDTR and TR-MOKE measurements of the 0.4 μm AlN epilayer with three types of transducers. Figure 4(b) shows the range of Λ and G that results in a good agreement between our data and the predictions of the model. For TDTR measurements with an 80 nm Al transducer (1600 ps), the data are consistent with Λ between 140 and $700 \text{ Wm}^{-1} \text{ K}^{-1}$. For TDTR measurements with the 40 nm TiN transducer ($\tau \approx 200 \text{ ps}$), Λ can be restricted to a narrower range of values between 100 and $260 \text{ Wm}^{-1} \text{ K}^{-1}$. Finally, TR-MOKE data collected with the 7 nm PtCo/TiN transducer ($\tau \approx 40 \text{ ps}$), implies Λ between 130 and $200 \text{ Wm}^{-1} \text{ K}^{-1}$. We conclude that Λ of the 0.4 μm AlN epilayer is $165 \pm 35 \text{ Wm}^{-1} \text{ K}^{-1}$.

The sensitivity of the TDTR and TR-MOKE signals to Λ and G is shown in Figs. 4(c)–4(e). This sensitivity analysis reveals two reasons why the PtCo/TiN transducer allows for a more accurate measurement of Λ . First, as expected, sensitivity to Λ of the thin AlN layer increases as τ of the transducer decreases. The maximum sensitivities to Λ for the Al ($\tau \approx 1300 \text{ ps}$), TiN ($\tau \approx 200 \text{ ps}$), and PtCo/TiN ($\tau \approx 40 \text{ ps}$), transducers are -0.1 , -0.3 , and -0.5 , respectively. Second, small τ allows for better differentiation between Λ and G . For the experiment with a PtCo/TiN transducer, the peak sensitivity to G and Λ occur at distinctly different time delays of 150 and 600 ps, respectively. As a result, G can be fixed by fitting to experimental signals collected at $\sim 150 \text{ ps}$. And, Λ can be fixed by fitting to signals collected at $\sim 600 \text{ ps}$. This is not possible for the experiment with an Al transducer because the maximum sensitivity to G and Λ both occur at a similar time delay of $\sim 3.5 \text{ ns}$.

In Fig. 5, we show the results of TR-MOKE measurements of the three AlN thin films. The thermal conductivity of the heteroepitaxial 1 μm AlN film on sapphire is $\Lambda \approx 300 \pm 70 \text{ Wm}^{-1} \text{ K}^{-1}$. This is in good agreement with Λ values of 270 to $370 \text{ Wm}^{-1} \text{ K}^{-1}$ typically reported for high purity bulk single crystals of AlN.^{32–34} The thermal conductivity of the heteroepitaxial 0.4 μm AlN film grown on sapphire is less: $\Lambda \approx 165 \pm 35 \text{ Wm}^{-1} \text{ K}^{-1}$. The reduced thermal conductivity in the heteroepitaxial 0.4 vs 1 μm AlN layers may be due to the tendency of heteroepitaxial films to have a high concentration of

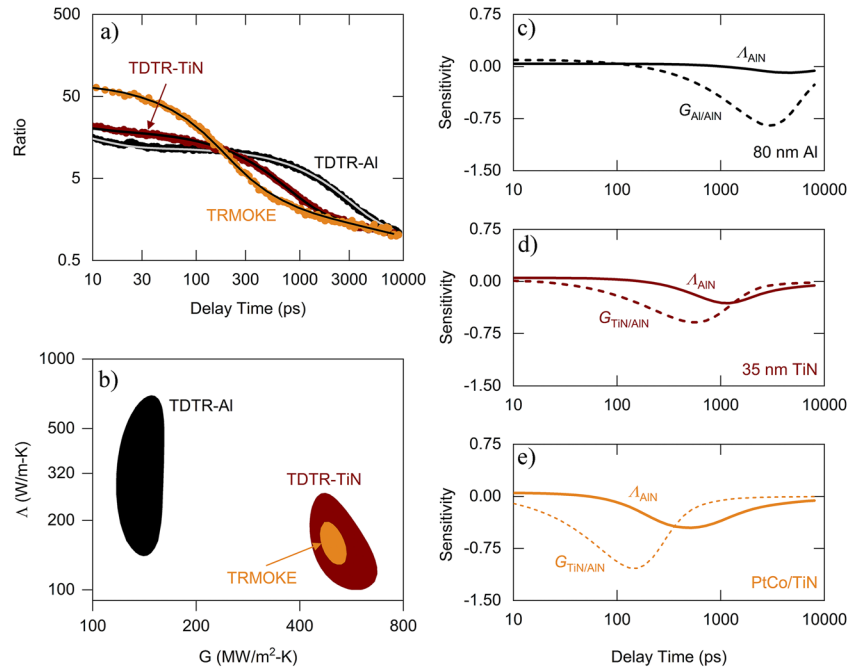


FIG. 4. Thermal conductivity measurements of $0.4 \mu\text{m}$ AlN thin film with different metal film transducers. (a) TRMOKE data (orange markers) and TDTR data with a 35 nm TiN transducer (burgundy markers) and an 80 nm Al transducer (black markers). Solid lines are best-fit predictions of the thermal model. (b) Contour plot showing the thermal conductivity and interface conductance values that produce good fits to the data in (a). A good fit is defined as having a root mean square percentage error $<6.5\%$. (c)–(e) Model predictions for the sensitivity of measured signals to the two fit parameters as a function of time delay.

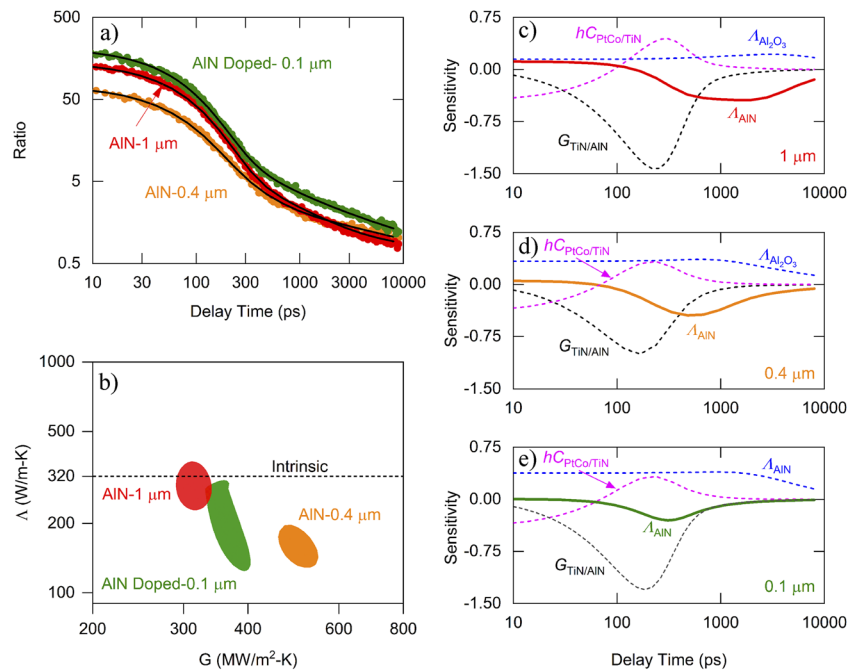


FIG. 5. (a) TR-MOKE data for the AlN- $1 \mu\text{m}$ film (red marker) the AlN- $0.4 \mu\text{m}$ film (orange marker), and the AlN Si-doped $0.1 \mu\text{m}$ film (green markers). Solid lines are best-fit predictions of the thermal model (b) Contour plot showing the thermal conductivity and interface conductance values that produce good fits to the data in (a). (c)–(e) Model predictions for how measured signals depend on the various thermal model parameters as a function of time delay.

24 August 2023 14:57:18

defects near the substrate interface. Or it may be due to differences in defect concentration due to different synthesis methods.

We now turn our attention to the Si-doped 0.1 μm AlN sample. When analyzing the TR-MOKE data for this sample, we simultaneously fit the interface conductance G , the thin film thermal conductivity, and the thermal conductivity of the bulk AlN substrate. We fit for Λ of the AlN substrate at a time delay of 10 ps, and for G and Λ of the thin film at longer time delays. At a delay time of 10 ps, the experimental signal is sensitive only to the substrate thermal conductivity, and the heat capacity per unit area of the PtCo/TiN transducer, $hC_{\text{PtCo/TiN}}$ [see Fig. 5(e)]. It has almost no sensitivity to G or Λ of the 0.1 μm AlN film. The best fit value for Λ of the AlN substrate is $285 \text{ W m}^{-1} \text{ K}^{-1}$, which is similar to values reported for bulk high purity single crystals.^{32–34}

The best-fit Λ value for the 0.1 μm AlN film is $\Lambda \approx 200 \text{ W m}^{-1} \text{ K}^{-1}$. However, with a thermal conductivity comparable to bulk AlN, and a thickness of 0.1 μm , the thermal resistance L/Λ of the AlN layer is less than $0.5 \text{ m}^2 \text{ K/GW}$. As a result, the experimental sensitivity of the MOKE signal to Λ of AlN film peaks at a fairly small value of -0.25 , see Fig. 5(e). This leads to significant uncertainty in our best-fit value for Λ of the Si-doped thin film. Without making any assumptions about the value of Λ for the AlN thin film relative to the bulk crystal, our TR-MOKE data are consistent with any Λ between 120 and 900 W/(mK) . However, we can further reduce our uncertainty by adding a constraint to our thermal model that Λ of the AlN layer is less than or equal to the AlN substrate. With this constraint, we conclude that the homoepitaxial 0.1 μm AlN layer has $\Lambda \approx 200 \pm 80 \text{ W/(mK)}$; see Fig. 5(b).

The best-fit value for the thermal conductivity of the 0.1 μm AlN film is comparable to the underlying AlN. So, we conclude that a Si doping concentration of 10^{19} cm^{-3} is not sufficiently high enough to suppress the thermal conductivity an amount more than our experimental uncertainties. Our results are consistent with other findings in the literature. For example, when Si films are doped with boron at a concentration level of $\sim 10^{19} \text{ cm}^{-3}$ the thermal conductivity is reduced by $\sim 20\%$.³⁵ Additionally, studies have reported that Si doping of GaN at a concentration of approximately $\sim 7 \times 10^{18} \text{ cm}^{-3}$ leads to a 17% reduction in GaN thermal conductivity.³⁶

VII. MINIMUM SUBSTRATE THICKNESS REQUIREMENTS FOR THERMAL CONDUCTIVITY MEASUREMENTS

Our experimental measurements above raise an interesting question. In general, how thick does a thin film need to be for TDTR or TR-MOKE to accurately measure its thermal conductivity? To answer this question, we performed an analysis using our thermal model. We use our analytical solution to the heat diffusion equation¹¹ to simulate the ratio for a system with the geometry of (transducer layer)/(thin film)/sapphire. We varied the thin-film thermal conductivity in our simulations to be $1 < \Lambda_{\text{film}} < 1000 \text{ W/(mK)}$. We also varied the thin-film thickness to be $3 \text{ nm} < L_{\text{film}} < 3 \mu\text{m}$. As a transducer layer, we consider an 80 nm Al transducer that is standard in TDTR experiments. We also consider the [1 nm-Pt/0.4 nm-Co]₃/[2 nm-TiN] transducer that was the focus of the current study. After simulating the ratio signal, we treat the simulated signal as data, and fit for the transducer/thin-film G and thin-film Λ .

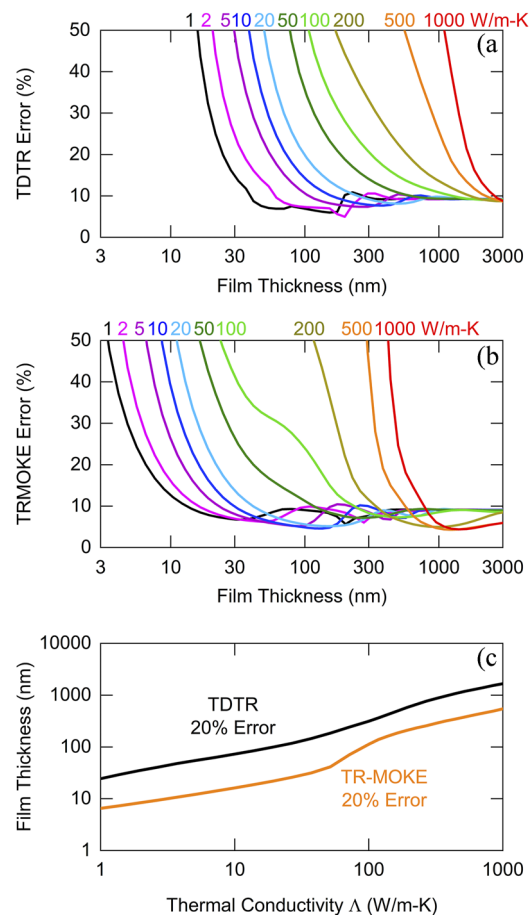


FIG. 6. Thermal model calculation of the expected error in (a) the TDTR and (b) the TR-MOKE experiments as a function of thin film thickness. Each curve shows the expected error for a material with the labeled thermal conductivity. (c) Predictions of the minimum film thickness required in order for a TDTR or TR-MOKE measurement to accurately characterize the film thermal conductivity. For materials with larger thermal conductivities, thicker films are required. TR-MOKE with a fast PtCo/TiN transducer can measure films 3–5 \times thinner than is possible with TDTR and an 80 nm Al transducer.

To mimic uncertainty in thermal model parameters that exists in real experiments, we used slightly different parameters for fitting the data than we used to simulate the data. We performed three fits to the data. One with the transducer thickness set to be in error by 5%. One with the thin-film thickness set to be in error by 5%. One with the thermal conductivity of the substrate set to be in error by 5%. We define the fit error for each of these trials to be $\delta = \Lambda_{\text{fit}}/\Lambda_{\text{film}}$. Finally, the total error is calculated by adding the results from the three trials in quadrature. The total error vs film thickness is shown in Fig. 6. As expected, the error is lower in all cases for TR-MOKE with a PtCo/TiN transducer than TDTR with an Al transducer.

VIII. CONCLUSION

In conclusion, we used TR-MOKE to study the cross-plane Λ of AlN thin films with thicknesses of 1, 0.4, and 0.1 μm . We maximized the spatiotemporal resolution of our pump/probe measurement by

using a thin magnetic multilayer transducer of PtCo/TiN. The TiN interfacial layer maximizes G between the transducer and the substrate. The small overall thickness of ~ 7 nm minimizes the thermal mass of the transducer and allows for a thermal response time $\sim 30\times$ faster than the 80 nm Al transducer used in most TDTR experiments. The thermal response time of the transducer has a strong effect on the sensitivity of our measurement to transport near the sample surface. We were then able to bound the thermal conductivities of the AlN thin films as follows: the thermal conductivity of the heteroepitaxial $1\ \mu\text{m}$ AlN film on sapphire is $\Lambda \approx 300 \pm 70\ \text{Wm}^{-1}\ \text{K}^{-1}$. The thermal conductivity of the heteroepitaxial $0.4\ \mu\text{m}$ AlN film grown on sapphire is $\Lambda \approx 165 \pm 35\ \text{Wm}^{-1}\ \text{K}^{-1}$. The thermal conductivity of the homoepitaxial $0.1\ \mu\text{m}$ n-type AlN layer is $\Lambda \approx 200 \pm 80\ \text{W/(mK)}$. Finally, we calculated the minimum film thicknesses required for TDTR and TR-MOKE to accurately measure the thermal conductivity of thin films with varied thermal conductivity. Our modeling shows that to accurately characterize transport in thin films with Λ of 1, 100, and 1000 W/mK, TDTR with an 80 nm Al transducer requires the thin films to have a minimum thickness of 25, 300, and 1600 nm, respectively. Alternatively, for TR-MOKE with an ultrafast PtCo/TiN transducer, the films can be as thin as ~ 10 , 100, and 500 nm, respectively. This work has presented a novel approach for accurate thermal transport measurements of low thermal resistance films and structures. This advance fills a gap that existed in the types of materials and structures that could be characterized by pump/probe nanoscale heat transfer metrologies.

SUPPLEMENTARY MATERIAL

See the supplementary material for details of RMSE analysis and fitting results of control samples measured by TR-MOKE.

ACKNOWLEDGMENTS

This research was supported as part of ULTRA, an Energy Frontier Research Center, funded by the U.S. Department of Energy (DOE), Office of Science, Basic Energy Sciences (BES) (Award No. DE-SC0021230).

AUTHOR DECLARATIONS

Conflict of Interest

The authors have no conflicts to disclose.

Author Contributions

Frank Angeles: Writing – original draft (equal). **Samreen Khan:** Data curation (equal). **Victor H. Ortiz:** Methodology (supporting). **Mingfei Xu:** Resources (equal). **Shisong Luo:** Resources (equal). **Dinusha Herath Mudiyanse:** Resources (equal). **Houqiang Fu:** Resources (equal). **Yuji Zhao:** Resources (equal); Writing – review & editing (supporting); **Richard B. Wilson:** Supervision (equal); Visualization (equal); Writing – original draft (equal); Writing – review & editing (equal).

DATA AVAILABILITY

The data that support the findings of this study are available from the corresponding author upon request.

REFERENCES

- J. Y. Tsao, S. Chowdhury, M. A. Hollis, D. Jena, N. M. Johnson, K. A. Jones, R. J. Kaplar, S. Rajan, C. G. Van de Walle, E. Bellotti, C. L. Chua, R. Collazo, M. E. Coltrin, J. A. Cooper, K. R. Evans, S. Graham, T. A. Grotjohn, E. R. Heller, M. Higashiwaki, M. S. Islam, P. W. Juodawlkis, M. A. Khan, A. D. Koehler, J. H. Leach, U. K. Mishra, R. J. Nemanich, R. C. N. Pilawa-Podgurski, J. B. Shealy, Z. Sitar, M. J. Tadjer, A. F. Witulski, M. Wraback, and J. A. Simmons, "Ultrawide-bandgap semiconductors: Research opportunities and challenges," *Adv. Electron. Mater.* **4**, 1600501 (2018).
- A. Hickman *et al.*, "High breakdown voltage in RF AlN/GaN/AlN quantum well HEMTs," *IEEE Electron Device Lett.* **40**(8), 1293–1296 (2019).
- T. Wei, *et al.*, "GaN/AlN quantum-disk nanorod 280 nm deep ultraviolet light emitting diodes by molecular beam epitaxy," *Optics Lett.* **40**(1), 121–124 (2015).
- C. E. Green, A. G. Fedorov, and Y. K. Joshi, "Scaling analysis of performance trade-offs in electronics cooling," *Proceedings of the ASME InterPack Conference 2009, IPACK2009* (ASME, 2010), Vol. 2, No. 4, pp. 1047–1056.
- E. Pop, "Energy dissipation and transport in nanoscale devices," *Nano Res.* **3**, 147–169 (2010).
- Z. Cheng, Y. R. Koh, A. Mamun, J. Shi, T. Bai, K. Huynh, L. Yates, Z. Liu, R. Li, E. Lee, M. E. Liao, Y. Wang, H. M. Yu, M. Kushimoto, T. Luo, M. S. Goorsky, P. E. Hopkins, H. Amano, A. Khan, and S. Graham, "Experimental observation of high intrinsic thermal conductivity of AlN," *Phys. Rev. Mater.* **4**, 044602 (2020).
- Y. R. Koh, Z. Cheng, A. Mamun, M. S. Bin Hoque, Z. Liu, T. Bai, K. Hussain, M. E. Liao, R. Li, J. T. Gaskins, A. Giri, J. Tomko, J. L. Braun, M. Gaevski, E. Lee, L. Yates, M. S. Goorsky, T. Luo, A. Khan, S. Graham, and P. E. Hopkins, "Bulk-like intrinsic phonon thermal conductivity of micrometer-thick AlN films," *ACS Appl. Mater. Interfaces* **12**, 29443–29450 (2020).
- L. Shi, D. Li, C. Yu, W. Jang, D. Kim, Z. Yao, P. Kim, and A. Majumdar, "Measuring thermal and thermoelectric properties of one-dimensional nanostructures using a microfabricated device," *J. Heat Transfer* **125**, 881–888 (2003).
- I. Jo, M. T. Pettes, J. Kim, K. Watanabe, T. Taniguchi, Z. Yao, and L. Shi, "Thermal conductivity and phonon transport in suspended few-layer hexagonal boron nitride," *Nano Lett.* **13**, 550–554 (2013).
- V. Singh, T. L. Bougher, A. Weathers, Y. Cai, K. Bi, M. T. Pettes, S. A. McMenamin, W. Lv, D. P. Resler, T. R. Gattuso, D. H. Altman, K. H. Sandhage, L. Shi, A. Henry, and B. A. Cola, "High thermal conductivity of chain-oriented amorphous polythiophene," *Nat. Nanotechnol.* **9**, 384–390 (2014).
- D. G. Cahill, "Analysis of heat flow in layered structures for time-domain thermoreflectance," *Rev. Sci. Instrum.* **75**, 5119–5122 (2004).
- R. B. Wilson, B. A. Apgar, L. W. Martin, and D. G. Cahill, "Thermoreflectance of metal transducers for optical pump-probe studies of thermal properties," *Opt. Express* **20**, 28829–28838 (2012).
- J. Kimling, A. Philippi-Kobs, J. Jacobsohn, H. P. Oepen, and D. G. Cahill, "Thermal conductance of interfaces with amorphous SiO₂ measured by time-resolved magneto-optic Kerr-effect thermometry," *Phys. Rev. B* **95**, 184305 (2017).
- D. S. Katzer and M. Cardona, "Thermal-conductivity measurements of GaAs/AlAs superlattices using a picosecond optical pump-and-probe technique," *Phys. Rev. B* **59**, 8105–8113 (1999).
- D. H. Olson, J. L. Braun, and P. E. Hopkins, "Spatially resolved thermoreflectance techniques for thermal conductivity measurements from the nanoscale to the mesoscale," *J. Appl. Phys.* **126**, 150901 (2019).
- C. Yuan, B. Meng, Y. Mao, M. Wu, F. Jia, L. Yang, X. Ma, and Y. Hao, "Transducer-less thermoreflectance technique for measuring thermal properties of the buried buffer layer and interface in GaN-based HEMTs," *ACS Appl. Electron. Mater.* **45**, 984–995 (2022).

- ¹⁷S. Warkander and J. Wu, “Transducerless time domain reflectance measurement of semiconductor thermal properties,” *J. Appl. Phys.* **2**, 025101 (2022).
- ¹⁸J. Liu, G. M. Choi, and D. G. Cahill, “Measurement of the anisotropic thermal conductivity of molybdenum disulfide by the time-resolved magneto-optic Kerr effect,” *J. Appl. Phys.* **116**, 233107 (2014).
- ¹⁹E. Beaurepaire, J.-C. Merle, A. Daunois, and J.-Y. Bigot, “Ultrafast spin dynamics in ferromagnetic nickel,” *Phys. Rev. Lett.* **76**, 4250–4253 (1996).
- ²⁰J. P. Feser, J. Liu, and D. G. Cahill, “Pump-probe measurements of the thermal conductivity tensor for materials lacking in-plane symmetry,” *Rev. Sci. Instrum.* **85**, 104903 (2014).
- ²¹F. Kargar, E. A. Coleman, S. Ghosh, J. Lee, M. J. Gomez, Y. Liu, A. S. Magana, Z. Barani, A. Mohammadzadeh, B. Debnath, R. B. Wilson, R. K. Lake, and A. A. Balandin, “Phonon and thermal properties of quasi-two-dimensional FePS₃ and MnPS₃ antiferromagnetic semiconductors,” *ACS Nano* **14**, 2424–2435 (2020).
- ²²J. Zhu, H. Park, J. Y. Chen, X. Gu, H. Zhang, S. Karthikeyan, N. Wendel, S. A. Campbell, M. Dawber, X. Du, M. Li, J. P. Wang, R. Yang, and X. Wang, “Revealing the origins of 3D anisotropic thermal conductivities of black phosphorus,” *Adv. Electron. Mater.* **2**, 1600040 (2016).
- ²³S. Khan, F. Angeles, J. Wright, S. Vishwakarma, V. H. Ortiz, E. Guzman, F. Kargar, A. A. Balandin, D. J. Smith, D. Jena, and H. G. Xing, “Properties for thermally conductive interfaces with wide-bandgap materials,” *ACS Appl. Mater. Interfaces* **14**, 36178–36188 (2022).
- ²⁴R. M. Costescu, M. A. Wall, and D. G. Cahill, “Thermal conductance of epitaxial interfaces,” *Phys. Rev. B* **67**, 054302 (2003).
- ²⁵H. Fu, X. Huang, H. Chen, Z. Lu, and Y. Zhao, “Fabrication and characterization of ultra-wide bandgap AlN-based Schottky diodes on sapphire by MOCVD,” *IEEE J. Electron Devices Soc.* **5**, 518–524 (2017).
- ²⁶H. Fu, I. Baranowski, X. Huang, H. Chen, Z. Lu, J. Montes, X. Zhang, and Y. Zhao, “Demonstration of AlN Schottky barrier diodes with blocking voltage over 1 kV,” *IEEE Electron Device Lett.* **38**, 1286–1289 (2017).
- ²⁷M. J. Gomez, K. Liu, J. G. Lee, and R. B. Wilson, “High sensitivity pump-probe measurements of magnetic, thermal, and acoustic phenomena with a spectrally tunable oscillator,” *Rev. Sci. Instrum.* **91**, 023905 (2020).
- ²⁸F. Angeles, X. Shi, and R. B. Wilson, “*In situ* and *ex situ* processes for synthesizing metal multilayers with electronically conductive interfaces,” *J. Appl. Phys.* **131**, 225302 (2022).
- ²⁹H. Jang, L. Marnitz, T. Huebner, J. Kimling, T. Kuschel, and D. G. Cahill, “Thermal conductivity of oxide tunnel barriers in magnetic tunnel junctions measured by ultrafast thermoreflectance and magneto-optic Kerr effect thermometry,” *Phys. Rev. Appl.* **13**, 024007 (2020).
- ³⁰B. C. Gundrum, D. G. Cahill, and R. S. Averback, “Thermal conductance of metal-metal interfaces,” *Phys. Rev. B* **72**, 245426 (2005).
- ³¹N. K. Ravichandran and D. Broido, “Unified first-principles theory of thermal properties of insulators,” *Phys. Rev. B* **98**, 085205 (2018).
- ³²G. A. Slack, R. A. Tanzilli, R. O. Pohl, and J. W. Vandersande, “The intrinsic thermal conductivity of AlN,” *J. Phys. Chem. Solids* **48**, 641–647 (1987).
- ³³R. Rounds, *et al.*, “Thermal conductivity of single-crystalline AlN,” *Appl. Phys. Express* **11**(7), 071001 (2018).
- ³⁴R. Rounds, *et al.*, “The influence of point defects on the thermal conductivity of AlN crystals,” *J. Appl. Phys.* **123**(18), 185107 (2018).
- ³⁵R. B. Wilson and D. G. Cahill, “Anisotropic failure of Fourier theory in time-domain thermoreflectance experiments,” *Nat. Commun.* **5**, 5075 (2014).
- ³⁶P. P. Paskov, M. Slomski, J. H. Leach, J. F. Muth, and T. Paskova, “Effect of Si doping on the thermal conductivity of bulk GaN at elevated temperatures—theory and experiment,” *AIP Adv.* **7**, 095302 (2017).